Research Article Vol. 5, No. 3 / March 2018 / Optica 237

Tabletop nonlinear optics in the 100-eV spectral region

B. Bergues,[1,2,8,†] D. E. Rivas,[1,2,7,†] M. Weidman,[1,†] A. A. Muschet,[1,3,†] W. Helml,[2] A. Guggenmos,[1,2] V. Pervak,[1,2] U. Kleineberg,[1,2] G. Marcus,[1,5] R. Kienberger,[1,4] D. Charalambidis,[6] P. Tzallas,[6] H. Schröder,[1] F. Krausz,[1,2] and L. Veisz[1,3,*]

[1]Max-Planck-Institut für Quantenoptik, Hans-Kopfermann Strasse 1, 85748 Garching, Germany
[2]Fakultät für Physik, Ludwig-Maximilians-Universität München, Am Coulombwall 1, 85748 Garching, Germany
[3]Department of Physics, Umeå University, SE-901 87 Umeå, Sweden
[4]Physics Department, Technische Universität München, James-Frank-Str. 1, 85748 Garching, Germany
[5]Department of Applied Physics, the Benin School of Engineering and Computer Science, The Hebrew University of Jerusalem, Jerusalem, 91904, Israel
[6]Foundation for Research and Technology-Hellas, Institute of Electronic Structure and Laser, P.O. Box 1527, GR-711 10 Heraklion, Crete, Greece
[7]Current address: ICFO - The Institute of Photonic Sciences, Av. Carl Friedrich Gauss, 3, 08860 Castelldefels, Barcelona, Spain
[8]e-mail: boris.bergues@mpq.mpg.de
*Corresponding author: laszlo.veisz@umu.se

Received 8 November 2017; revised 18 January 2018; accepted 19 January 2018 (Doc. ID 312912); published 23 February 2018

Nonlinear light–matter interactions in the extreme ultraviolet (XUV) are a prerequisite to perform XUV-pump/XUV-probe spectroscopy of core electrons. Such interactions are now routinely investigated at free-electron laser (FEL) facilities. Yet, electron dynamics are often too fast to be captured with the femtosecond resolution of state-of-the-art FELs. Attosecond pulses from laser-driven XUV-sources offer the necessary temporal resolution. However, intense attosecond pulses supporting nonlinear processes have only been available for photon energy below 50 eV, precluding XUV-pump/XUV-probe investigation of typical inner-shell processes. Here, we surpass this limitation by demonstrating two-photon absorption from inner electronic shells of xenon at photon energies around 93 eV and 115 eV. This advance opens the door for attosecond real-time observation of nonlinear electron dynamics deep inside atoms.

OCIS codes: (020.4180) Multiphoton processes; (340.7480) X-rays, soft x-rays, extreme ultraviolet (EUV); (140.7240) UV, EUV, and X-ray lasers.

https://doi.org/10.1364/OPTICA.5.000237

1. INTRODUCTION

Nonlinear photoionization triggered by high-intensity free-electron laser (FEL) pulses has opened new horizons for the investigation of inner-shell electron dynamics in atomic and molecular systems [1]. The pioneering studies on multi-photon ionization (MPI) of xenon atoms at 93 eV provided a particularly impressive example of the richness of MPI dynamics [2,3]. In these studies, ionic charge states up to Xe^{21+} were observed, involving the absorption of at least 57 photons. Xenon is a model system for collective inner-shell electron dynamics involving a giant dipole resonance [4]. These dynamics in xenon turned out to be much richer than expected and have been the subject of numerous studies [5,6]. In particular, recent studies revealed that the giant 4d-ϵf dipole resonance in xenon is in fact composed of two short-lived resonances [7,8]. Apart from xenon, a number of other systems such as the elements Ba and La exhibit a giant resonance around 100 eV [9,10]. Since the latter is preserved in molecules containing them, the range of applications extends to molecules, clusters, fullerenes, or quantum dots [11].

The availability of attosecond pulses with a photon energy around 100 eV with sufficient intensity to support multi-photon interactions, would allow time resolving of such collective inner-shell dynamics [12,13]. When the duration of the extreme ultraviolet (XUV) pulses is significantly shorter than the time scale of the autoionization process that follows the absorption of the first photon, the second photon interacts with a non-relaxed system. As a consequence, sequential ionization via a relaxed intermediate state is expected to be strongly inhibited in the attosecond regime. This contrasts with the femtosecond regime of FEL pulses for which sequential ionization prevails [14].

While FELs are potentially capable of producing pulses shorter than 1 fs [15,16], these pulses develop stochastically, and their timing cannot presently be precisely controlled. By contrast, high-harmonic generation (HHG) [17,18] driven by laser pulses with a controlled waveform [19] allows the reliable and reproducible generation of isolated attosecond pulses [20]. Until now, however, the low pulse energies provided by these sources has greatly hampered their use for nonlinear inner-shell excitation.

Second-order MPI processes have been observed at photon energies up to 50 eV with HHG-based sources, using gas [21–25] and over-dense plasma targets [26]. However, for most atomic species, these photon energies are insufficient for MPI of inner-shell electrons.

Microscopically, HHG in gaseous media is understood in terms of the recollision model [27,28]. As a collective process of many atoms, the HHG yield depends on macroscopic propagation effects, i.e., phase matching of the driving laser and the emitted harmonics in the gas medium. Experimentally, the optimum pulse energy is achieved with a multi-dimensional optimization of different generation parameters [29], such as gas pressure, interaction length, focus position with respect to the gas target, and laser intensity. The infrared (IR)-to-XUV conversion efficiency rapidly decreases towards shorter XUV wavelengths as a result of the decreasing single-atom response, increasing phase-matching sensitivity, and dispersion due to increasing ionization. Hence, the generation of intense XUV pulses at higher photon energies is ever more challenging. Despite efforts to optimize the XUV pulse energy using millijoule (mJ)-scale few-cycle pulses [30,31], a substantial increase is needed for the investigation of multiphoton processes at 100 eV.

In this paper, we report on two-photon multiple ionization of Xe at photon energies around 93 eV and 115 eV. We thereby demonstrate nonlinear interactions with an inner electronic shell (i.e., the 4d electronic shell of xenon). Moreover, we determine the two-photon ionization cross sections for this process. This progress is allowed by a 100-fold increase in the XUV pulse energy, utilizing the quadratic scaling of the harmonic yield with the diameter of the interaction region [32–34]. A novel scheme for broadband amplification of sub-two-cycle laser pulses towards multi-terawatt (multi-TW) peak power allows us to maintain the driving laser intensity at the required level in a much larger focus.

2. EXPERIMENTAL SETUP

The HHG process is driven by a multi-TW optical parametric synthesizer, the "Light Wave Synthesizer 20" (LWS-20), which delivers sub-two-cycle 75 mJ pulses with a central wavelength around 740 nm at a repetition rate of 10 Hz [35]. Up to 40 mJ of the pulse energy are used on target. With this pulse energy, a peak intensity above 10^{15} W/cm^2 is reached in a focal spot with 365 μm full width at half-maximum (FWHM). For the focusing (see Fig. 1), we use a 17 m focal-length spherical mirror (f# 340) that is preceded by an adaptive mirror to ensure a sufficient wave-front quality.

The generated XUV pulses typically exhibit a cutoff photon energy of about 125 eV. In the cutoff region, continuous and modulated single-shot spectra are observed, which are attributed to random shot-to-shot changes of the carrier-envelope phase of the driving laser pulses [35]. The XUV pulse energy within the Zr filter spectral transmission window that opens at 65 eV [Fig. 1(b)] can be as high as 40 nJ, corresponding to an IR-to-XUV energy conversion efficiency from the fundamental to photon energies >65 eV of the order of 10^{-6} [see Supplement 1]. This two-order-of-magnitude pulse energy increase with respect to state-of-the-art kilohertz (kHz) few-cycle systems [31] satisfies the expected energy scaling for high-energy few-cycle sources.

The beamline shown in Fig. 1 accommodates a tight refocusing of the XUV beam in the experimental chamber. After an expansion length of 14 m, an XUV mirror with a focal length of 125 mm is used to focus the XUV pulses on axis into a xenon gas

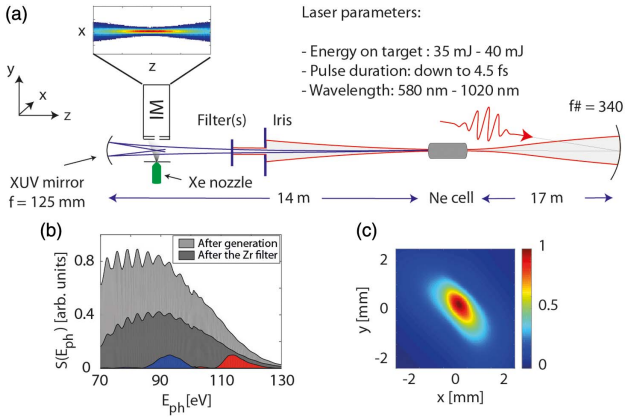

Fig. 1. Experimental setup. The LWS-20 laser system that drives the HHG delivers sub-two-cycle laser pulses with a central wavelength around 740 nm at a repetition rate of 10 Hz. The pulses propagate in a 35-m-long evacuated beamline where they are focused into the generation chamber to a focal spot of 365 μm FWHM using an $f = 17$ m spherical mirror. The XUV pulses are generated in a gas cell filled with a few mbar of neon. Optimum XUV pulses are typically generated with 35 mJ to 40 mJ laser pulse energy on target, providing a peak intensity of 1–3 × 10^{15} W/cm^2. After HHG, the XUV and laser pulses propagate collinearly to the entrance of the experimental chamber. There, one or two 150-nm-thick Zr filters can be inserted into the beam to block photons with an energy below 65 eV, including the driving laser radiation. A multilayer XUV mirror is used to focus the beam on axis onto a xenon gas jet located in the object plane of an ion microscope. The latter records the spatial distribution of ions produced in the XUV focus via photoionization of the target gas. The chamber is equipped with different single-shot XUV diagnostic devices (an XUV CCD camera, an XUV flat-field grating spectrometer, and an absolutely calibrated XUV photodiode), which are used to characterize the generated radiation. (b) 100-shot average of the spectral energy density $S(E_{ph})$ as a function of the photon energy E_{ph} after generation (light grey area), and after a 150-nm-thick Zr filter (dark grey area). The normalized XUV spectrum on target after reflection from the 93-eV (115-eV) XUV focusing mirror is indicated by the blue (red) area. For visual convenience, the maximum of the blue and red spectra have been normalized to the value 0.1. (c) XUV beam profile measured at the XUV mirror position and averaged over 100 shots.

target where different ionic charge states are generated via XUV photoionization. The present geometry performs a 110:1 imaging of the XUV source onto the target. Two different homemade multilayer XUV mirrors [36] with 10-eV bandwidth centered at 93 eV and 115 eV and a peak reflectivity of 16% [Fig. 1(b)] are used in this study. A typical XUV-beam profile at the XUV mirror is shown in Fig. 1(c). From the spectral intensity reflected by the XUV mirror, we estimate a Fourier limited XUV pulse duration of about 170 as (at FWHM) in both cases.

3. RESULTS

In order to explore the interaction of the XUV pulse with the target gas, we use an ion microscope (IM) [37–39] to record the spatial distribution of the different photo ions in the XUV focus. More specifically, the IM records the y-projection of the ion distribution as a function of their time of flight (TOF) with single-ion sensitivity. The XUV pulse energy on target amounts to 0.5 nJ ± 0.15 nJ and 0.25 nJ ± 0.06 nJ for the 93-eV and 115-eV experiments, respectively (see Supplement 1).

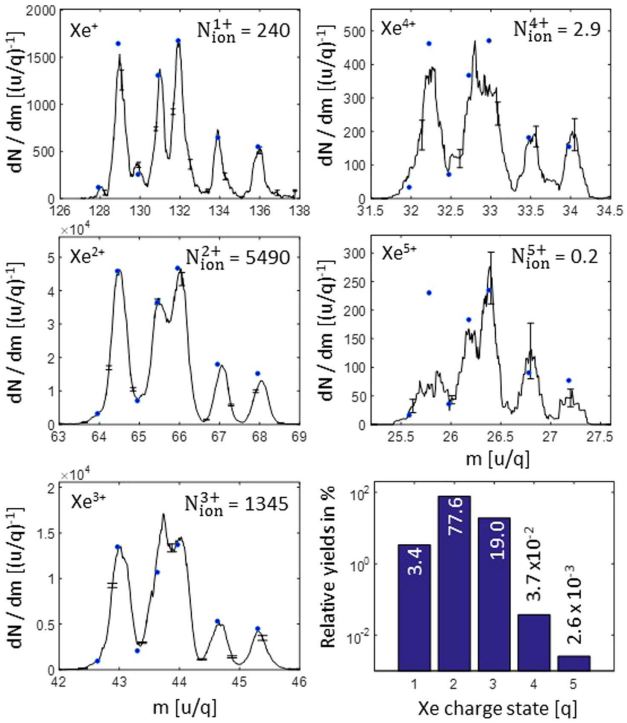

Fig. 2. TOF spectra of Xe at 93 eV. Measured mass spectra of the xenon charge states Xe^{q+} ($q = 1, \ldots, 5$) generated by photoionization of xenon atoms in the focus of the 93-eV XUV beam. The signal corresponds to the number of ions per unit mass-to-charge ratio m detected in a field of view of 395 μm in diameter. The number N_{ion}^{q+} in the right upper corner of each graph corresponds to the number of ions Xe^{q+} generated per shot in the field of view of the IM, taking into account the 50% detection efficiency. The blue markers indicate the expected positions and frequencies of the seven stable xenon isotopes. The relative photoionization yields of all the measured charge states are shown in the lower right panel.

In the ion TOF spectra measured using 93-eV XUV pulses (Fig. 2), the xenon charge states Xe^{q+} with $q = 1-3$ can be reached by the absorption of a single photon. The measured single-photoionization yield distribution, which results from different Auger decay paths of excited xenon hole states to different final ionic charge states, is in agreement with the literature [40]. In order to generate the observed charge states Xe^{4+} and Xe^{5+} with a threshold energy of 107.4 eV ± 0.8 eV and 160.8 eV ± 3.7 eV, respectively [41], at least two photons have to be absorbed. The intensity scaling for the Xe^{4+} production follows I^n with $n = 2.05 \pm 0.13$ (see Supplement 1), in accordance with a two-photon absorption process.

In order to determine the two-photon ionization cross section $\tilde{\sigma}^{(2)}$, we recall that a beam with a Gaussian profile and a certain M^2 parameter $\tilde{\sigma}^{(2)}$ can be expressed as (see Supplement 1)

$$\tilde{\sigma}^{(2)} = \frac{\lambda}{\pi} \times \frac{M^2}{N_{ph}^2} \times \frac{N_{tot}^{(2)}}{\rho_a}, \quad (1)$$

where ρ_a is the target gas density, $N_{tot}^{(2)}$ the total (time-integrated) number of two-photon ionization events integrated over the whole focal volume, N_{ph} the number of photons on target, and λ the XUV wavelength. Here $\tilde{\sigma}^{(2)}$ is defined as $Y^{(2)} = \tilde{\sigma}^{(2)} \times F^2$, where F is the photon fluence (number of photons per area) and $Y^{(2)}$ the two-photon ionization yield. It is worth noting that for a beam with a Gaussian profile and a certain M^2 parameter, $N_{tot}^{(2)}$ is independent of the focal geometry, but is inversely proportional to the M^2 factor of the XUV beam, which emphasizes the importance of the XUV-beam quality. By setting $M^2 = 1$ in Eq. (1), and assuming that the Xe^{4+} channel yields the main contribution to the second-order process, we can infer lower limits of $\tilde{\sigma}^{(2)} > (7.3 \pm 3.5) \times 10^{-36}$ cm^4 and $\tilde{\sigma}^{(2)} > (2.9 \pm 1.4) \times 10^{-36}$ cm^4 for the 93-eV and 115-eV experiments, respectively.

The IM images of the spatial distributions of $^{131}Xe^{2+}$ and $^{131}Xe^{4+}$ ($^{131}Xe^{3+}$ and $^{131}Xe^{4+}$) ions in the XUV focus that were recorded in the 93-eV (115-eV) experiment (Fig. 3) allow us to characterize the XUV focus and determine the photon fluence on target. Each image is composed of multiple measurements at different z positions, which permits a measurement over a longer z

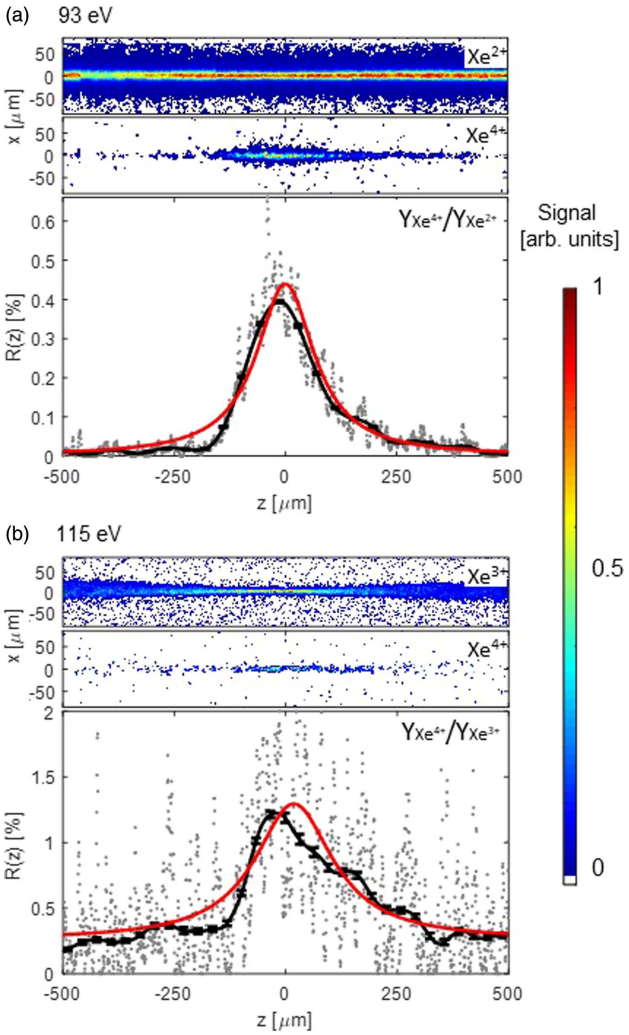

Fig. 3. Spatial dependence of the linear and nonlinear photoionization yields along the propagation axis z at a photon energy of (a) 93 eV and (b) 115 eV. Each of the images shown in the upper two panels in (a) and (b) correspond to an ion microscope image of the charge state indicated in the upper right corner. The maximum signal in each image is normalized to 1. The yield ratios $R(z) = Y_{Xe^{4+}}(z)/Y_{Xe^{2+}}(z)$ and $R(z) = Y_{Xe^{4+}}(z)/Y_{Xe^{3+}}(z)$ are shown in the lower panel of (a) and (b), respectively, where $Y_{Xe^{2+}}(z)$, $Y_{Xe^{3+}}(z)$ and $Y_{Xe^{4+}}(z)$ are obtained by integrating the corresponding images along x (grey data points). The black line is obtained from the grey data points by a 65-point smoothing. The red line, from which we obtain the Rayleigh range z_R, is a fit of the function $k \times (1 + z^2/z_R^2)^{-1}$ to the data with fit parameters k and z_R.

range than the field of view of the IM. Well below the saturation intensity, the x- and y-integrated single-photon ionization yield is independent of z. In contrast, for a process of order 2, the x- and y-integrated yield is proportional to the photon fluence, i.e., inversely proportional to the beam area at that z position. Thus, assuming a Gaussian beam with a certain M^2 factor, we can determine for the 93-eV (115-eV) experiment the Rayleigh range $z_R = 93\ \mu m \pm 10\ \mu m$ ($z_R = 96\ \mu m \pm 15\ \mu m$) from the z-dependent yield ratio $R(z)$ of Xe^{4+} and Xe^{2+} (Xe^{4+} and Xe^{3+}) ions [see Fig 3]. The advantage of using the yield ratio rather than the nonlinear $^{131}Xe^{4+}$ yield alone is that any error due to a possible inhomogeneity in the IM detection will cancel out. A FWHM focal spot size of $d_0 = 1.1 \pm 0.2\ \mu m$ ($d_0 = 2.5 \pm 0.45\ \mu m$) is determined from the measured beam divergence and the Rayleigh range (see Supplement 1). For the measured focus diameter of 1.1 μm (FWHM) and the measured pulse energy on target of 0.5 nJ, one would obtain an XUV intensity of $1.0 \times 10^{14}\ W/cm^2$, assuming a temporal intensity envelope with a FWHM 340 as, which corresponds to roughly twice the Fourier limited FWHM obtained from the XUV spectrum.

For the 115-eV experiment, both single-photon and two-photon absorption processes contribute to the Xe^{4+} yield, and the nonlinear contribution is 4.4 times larger at the focus [i.e., the signal at $z = 0\ \mu m$ compared to the signal at $z = -500\ \mu m$ in Fig. 3(b)]. The linear Xe^{4+}-yield contribution is consistent with the single-photon Xe^{4+} ionization cross section at 115 eV of $0.015 \times 10^{-18}\ cm^2$ [40].

For the 93-eV (115-eV) experiment, we determine the two-photon partial ionization cross section $\tilde{\sigma}^{(2)}$ for Xe^{4+} from the yield ratio R(0) of the Xe^{4+} and Xe^{2+} (Xe^{3+}) yields in the focus, the focus size d_0, the number of photons on target N_{ph}, and the partial single-photon ionization cross section σ for the production of Xe^{2+} (Xe^{3+}) ions,

$$\tilde{\sigma}^{(2)} = \frac{\pi\sigma}{2\ \ln(2)} \times \frac{d_0^2 \times R(0)}{N_{ph}}. \quad (2)$$

The experimental values obtained from Eqs. (1) and (2) are summarized in Table 1, where they are also compared to the predictions of the sequential ionization model, in which a first photon generates the ionic ground states of Xe^+, Xe^{2+}, and Xe^{3+}, from which a second photon is absorbed [14].

Table 1. Measured Xe^{4+} Two-Photon Ionization Cross Sections at 93 eV and 115 eV Determined Using Eqs. (1) and (2)[a]

	93 eV	115 eV
$\tilde{\sigma}^{(2)}_{Xe^{4+}}/(10^{-34}\ cm^4)$ [exp. Eq. (1)]	0.19 ± 0.09	2.0 ± 1.0
$\tilde{\sigma}^{(2)}_{Xe^{4+}}/(10^{-34}\ cm^4)$ [exp. Eq. (2)]	0.55 ± 0.27	4.9 ± 2.4
$\overline{\tilde{\sigma}^{(2)}_{Xe^{4+}}}/(10^{-34}\ cm^4)$ (exp. Mean)	0.37 ± 0.13	3.45 ± 1.2
$\tilde{\sigma}^{(2)}_{Xe^{4+}}/(10^{-34}\ cm^4)$ (theory)	2.6	1.36
$Y_{Xe^{4+}}/Y_{Xe^{5+}}$ (exp.)	14.5 ± 1.5	9 ± 2
$Y_{Xe^{4+}}/Y_{Xe^{5+}}$ (theory)	>61	1.4

[a]The average of the two measured values is compared to the predictions of the sequential ionization model. Also shown are the measured ratio of the nonlinear Xe^{4+} and Xe^{5+} yields and the corresponding values expected from the sequential model. The theoretical two-photon ionization cross sections and yield ratios are calculated using experimental single-photon ionization cross sections data from the literature (see Supplement 1).

4. DISCUSSION

Before discussing the results, it is worth pointing out that for photon energies above the ionization potential of helium, two-photon ionization of a neutral target always occurs via a resonant intermediate state. A fundamental question is whether or not the second photon is absorbed before the relaxation of the system is complete—after the absorption of the first photon. Sequential ionization via a relaxed intermediate state provides a good description of FEL experiments in the femtosecond regime [14,42,43]. In the attosecond regime, in contrast, the finite lifetime of the transient intermediate state has to be accounted for. A proper description of the two-photon ionization process in this case requires an accurate treatment of the electron correlations in the presence of nonlinear effects. A recent overview about the state of such approaches can be found in Ref. [44].

The duration of the XUV pulses used in our experiment is short compared to the relaxation time of the excited 4d hole states into the Xe^{2+} (Xe^{3+}) charge states via Auger (cascaded Auger) processes [45]. While the decay time of the Auger process leading to Xe^{2+} amounts to 6.3 fs ± 0.2 and 5.9 fs ± 0.2 fs for the $4d_{3/2}$ and $4d_{5/2}$ holes, respectively [46], the Auger decay time from the excited Xe^{2+} state to the Xe^{3+} states amounts to 30.8 fs ± 1.4 fs [47]. Although an exact temporal characterization of the XUV pulse was not realized with the present setup, the nonlinear nature of the HHG process temporally confines the XUV pulse to a fraction of the driving laser pulse. Therefore, the observed two-photon absorption process is expected to occur on a time scale significantly shorter than the decay time of the excited 4d-hole state.

As can be seen in Table 1, the two-photon ionization cross sections reported in the present work are indeed not compatible with a sequential model. As compared to the model predictions, that assume sequential ionization via the relaxed ionic ground states, the measured two-photon ionization cross section of Xe^{4+} is 7 times smaller at 93 eV and 2.5 larger at 115 eV. This suggests that the generation of this charge state follows a different ionization pathway via the unrelaxed excited 4d-hole state. Similar discrepancies are observed for the measured ratio of the Xe^{4+} and Xe^{5+} ionization yields, a quantity independent of the XUV pulse energy. As compared to the predictions assuming sequential ionization via the relaxed ionic ground states, the measured ratio is more than 4 times smaller at 93 eV and 6.4 times larger at 115 eV. This again suggests that the absorption of the second photon in the short pulse regime occurs via a different pathway. As discussed above, the significant discrepancies of our experimental results with respect to the predictions of a sequential model indicate that our short pulse duration starts sensing the life time of the transient intermediate states. Future experimental and theoretical studies are needed to shed light on the exact nature of these processes that are now experimentally accessible.

5. CONCLUSION AND OUTLOOK

In summary, we have used an attosecond XUV source to investigate the absorption of two 100-eV photons within the giant resonance of xenon. We have observed distinct deviations with respect to FEL results, which originate from the shorter XUV pulse duration provided by our system. These differences are indicative of dynamics on a few-femtosecond time scale or even

shorter, which can be ideally interrogated using an attosecond XUV-pump/XUV-probe scheme.

Beyond the particular example of xenon, the 100-eV energy region allows reaching the absorption edge of a variety of elements, including Al, Be, and Si. Besides the study of giant resonances, other experiments such as two-color pump-probe investigations in He call for intense attosecond radiation around 100 eV [48]. Higher photon energies ranging into the water window would allow time-resolved measurements in organic molecules. Such a possibility would result in unprecedented applications in biology and chemical science.

Our proof-of-principle experiment opens the door for such studies by demonstrating the capability of few-cycle-driven high-harmonic sources to combine extreme temporal confinement with peak powers required for observing nonlinear interactions. The feasibility of this energy scaling is expected to motivate efforts towards the development of next-generation high-intensity attosecond sources [49] and paves the way for the real-time exploration of so far unresolved inner-shell electron dynamics.

Funding. Project Transregio TR18, Deutsche Forschungsgemeinschaft (DFG); Munich Centre for Advanced Photonics (MAP); Euratom research and training program 2014-2018, FP7 Fusion Energy Research (EURATOM-FUSION) within the framework of the EUROfusion Consortium (633053); H2020 European Research Council (ERC); Laserlab-Europe (MPQ002119).

Acknowledgment. We are grateful for fruitful discussions with Wolfgang Schweinberger, Florian Siegrist, Nicholas Karpowicz, Piotr Matyba, and Eleftherios Goulielmakis. We further acknowledge the technical support offered by Harald Haas, Anton Horn, Tobias Kleinhenz, Walter Ritt, and Manfred Fischer. B. B. acknowledges additional support from Matthias Kling.

See Supplement 1 for supporting content.

†These authors contributed equally for this work.

REFERENCES

1. J. Ullrich, A. Rudenko, and R. Moshammer, "Free-electron lasers: new avenues in molecular physics and photochemistry," Annu. Rev. Phys. Chem. **63**, 635–660 (2012).
2. A. A. Sorokin, S. V. Bobashev, T. Feigl, K. Tiedtke, H. Wabnitz, and M. Richter, "Photoelectric effect at ultra-high intensities," Phys. Rev. Lett. **99**, 213002 (2007).
3. M. G. Makris, P. Lambropoulos, and A. Mihelic, "Theory of multiphoton multielectron ionization of xenon under strong 93-eV radiation," Phys. Rev. Lett. **102**, 033002 (2009).
4. V. Schmidt, "Photoionization of atoms using synchrotron radiation," Rep. Prog. Phys. **55**, 1483–1659 (1992).
5. V. Richardson, J. T. Costello, D. Cubaynes, S. Düsterer, J. Feldhaus, H. W. van der Hart, P. Juranic, W. B. Li, M. Meyer, M. Richter, A. A. Sorokin, and K. Tiedke, "Two-photon inner-shell ionization in the extreme ultraviolet," Phys. Rev. Lett. **105**, 013001 (2010).
6. L.-W. Pi and A. F. Starace, "Potential barrier effects in two-photon ionization processes," Phys. Rev. A **82**, 053414 (2010).
7. Y.-J. Chen, S. Pabst, A. Karamatskou, and R. Santra, "Theoretical characterization of the collective resonance states underlying the xenon giant dipole resonance," Phys. Rev. A **91**, 032503 (2015).
8. T. Mazza, A. Karamatskou, M. Ilchen, S. Bakhtiarzadeh, A. J. Rafipoor, P. O'Keeffe, T. J. Kelly, N. Walsh, T. Costello, M. Meyer, and R. Santra, "Sensitivity of nonlinear photoionization to resonance substructure in collective excitation," Nat. Commun. **6**, 6799 (2015).
9. C. Sternemann, H. Sternemann, S. Huotari, F. Lehmkühler, M. Tolan, and J. S. Tse, "The barium giant dipole resonance in barite: a study of soft x-ray absorption edges using hard x-rays," J. Anal. At. Spectrom. **23**, 807–881 (2008).
10. U. Köble, L. Kiernan, J. T. Costello, J.-P. Mosnier, E. T. Kennedy, V. K. Ivanov, V. A. Kupchenko, and M. S. Shendrik, "4f (1P) giant dipole resonance in La^{3+}," Phys. Rev. Lett. **74**, 2188–2191 (1995).
11. M. Y. Amusia and J. P. Connerade, "The theory of collective motion probed by light," Rep. Prog. Phys. **63**, 41–70 (2000).
12. K. Midorikawa, Y. Nabekawa, and A. Suda, "XUV multiphoton processes with intense high-order harmonics," Prog. Quantum Electron. **32**, 43–88 (2008).
13. G. Sansone, L. Poletto, and M. Nisoli, "High-energy attosecond light sources," Nat. Photonics **5**, 655–663 (2011).
14. P. Lambropoulos, K. G. Papamihail, and P. Decleva, "Theory of multiple ionization of xenon under strong XUV radiation and the role of the giant resonance," J. Phys. B **44**, 175402 (2011).
15. W. Helml, A. R. Maier, W. Schweinberger, I. Grguras, P. Radcliffe, G. Doumy, C. Roedig, J. Gagnon, M. Messerschmidt, S. Schorb, C. Bostedt, F. Grüner, L. F. DiMauro, D. Cubaynes, J. D. Bozek, T. Tschentscher, J. T. Costello, M. Meyer, R. Coffee, S. Düsterer, A. L. Cavalieri, and R. Kienberger, "Measuring the temporal structure of few-femtosecond free-electron laser x-ray pulses directly in the time domain," Nat. Photonics **8**, 950–957 (2014).
16. S. Huang, Y. Ding, Y. Feng, E. Hemsing, Z. Huang, J. Krzywinksi, A. A. Lutman, A. Marinelli, T. J. Maxwell, and D. Zhu, "Generating single-spike hard x-ray pulses with nonlinear bunch compression in free-electron lasers," Phys. Rev. Lett. **119**, 154801 (2017).
17. A. McPherson, G. Gibson, H. Jara, U. Johann, T. S. Luk, I. A. McIntyre, K. Boyer, and C. K. Rhodes, "Studies of multiphoton production of vacuum-ultraviolet radiation in the rare gases," J. Opt. Soc. Am. B **4**, 595–601 (1987).
18. M. Ferray, A. L'Huillier, X. F. Li, L. A. Lompre, G. Mainfray, and C. Manus, "Multiple-harmonic conversion of 1064 nm radiation in rare gases," J. Phys. B **21**, L31–L35 (1988).
19. A. Baltuska, T. Udem, M. Uiberacker, M. Hentschel, E. Goulielmakis, C. Gohle, R. Holzwarth, V. S. Yakovlev, A. Scrinzi, T. W. Hänsch, and F. Krausz, "Attosecond control of electronic processes by intense light fields," Nature **421**, 611–615 (2003).
20. R. Kienberger, E. Goulielmakis, M. Uiberacker, A. Baltuska, V. Yakovlev, F. Bammer, T. Westerwalbesloh, U. Kleineberg, U. Heinzmann, M. Drescher, and F. Krausz, "Atomic transient recorder," Nature **427**, 817–821 (2004).
21. P. Tzallas, D. Charalambidis, N. A. Papadogiannis, K. Witte, and G. D. Tsakiris, "Second-order autocorrelation measurements of attosecond XUV pulse trains," J. Mod. Opt. **52**, 321–338 (2005).
22. P. Tzallas, E. Skantzakis, L. A. A. Nikolopoulos, G. D. Tsakiris, and D. Charalambidis, "Extreme-ultraviolet pump-probe studies of one femtosecond scale electron dynamics," Nat. Phys. **7**, 781–784 (2011).
23. Y. Nabekawa, Y. Furukawa, T. Okino, A. A. Eilanlou, E. J. Takahashi, K. Yamanouchi, and K. Midorikawa, "Sub-10-fs control of dissociation pathways in the hydrogen molecular ion with a few-pulse attosecond pulse train," Nat. Commun. **7**, 12835 (2016).
24. B. Manschwetus, L. Rading, F. Campi, S. Maclot, H. Coudert-Alteirac, J. Lahl, H. Wikmark, P. Rudawski, C. M. Heyl, B. Farkas, T. Mohamed, A. L'Huillier, and P. Johnsson, "Two-photon double ionization of neon using an intense attosecond pulse train," Phys. Rev. A **93**, 061402 (2016).
25. T. R. Barillot, P. Matia-Hernando, D. Greening, D. J. Walke, T. Witting, L. J. Frasinkski, J. P. Marangos, and J. W. G. Tisch, "Towards XUV pump-probe experiments in the femtosecond to sub-femtosecond regime: new measurement of the helium two-photon ionization cross-section," Chem. Phys. Lett. **683**, 38–42 (2017).
26. Y. Nomura, R. Hörlein, P. Tzallas, B. Dromey, S. Rykovanov, Z. Major, J. Osterhoff, S. Karsch, L. Veisz, M. Zepf, D. Charalambidis, F. Krausz, and G. D. Tsakiris, "Attosecond phase locking of harmonics emitted from laser-produced plasmas," Nat. Phys. **5**, 124–128 (2009).
27. P. B. Corkum, "Plasma perspective on strong field multiphoton ionization," Phys. Rev. Lett. **71**, 1994–1997 (1993).
28. K. C. Kulander, K. J. Schafer, and J. K. Krause, "Ionization and harmonic conversion," in *Super Intense Laser Atom Physics* (Springer, 1993).

29. P. Rudawski, C. M. Heyl, F. Brizuela, J. Schwenke, A. Persson, E. Mansten, R. Rakowski, L. Rading, F. Campi, B. Kim, P. Johnsson, and A. L'Huillier, "A high-flux high-order harmonic source," Rev. Sci. Instrum. **84**, 073103 (2013).
30. F. Ferrari, F. Calegari, M. Lucchini, C. Vozzi, S. Stagira, G. Sansone, and M. Nisoli, "High-energy isolated attosecond pulses generated by above-saturation few-cycle fields," Nat. Photonics **4**, 875–879 (2010).
31. M. Ossiander, F. Siegrist, V. Shirvanyan, R. Pazourek, A. Sommer, T. Latka, A. Guggenmos, S. Nagele, J. Feist, J. Burgerdörfer, R. Kienberger, and M. Schultze, "Attosecond correlation dynamics," Nat. Phys. **13**, 280–285 (2016).
32. E. Takahashi, Y. Nabekawa, T. Otsuka, M. Obara, and K. Midorikawa, "Generation of highly coherent submicrojoule soft x rays by high-order harmonics," Phys. Rev. A **66**, 021802 (2002).
33. S. Chatziathanasiou, S. Kahaly, E. Skantzakis, G. Sansone, R. Lopez-Martens, S. Haessler, K. Varju, G. D. Tsakiris, D. Charalambidis, and P. Tzallas, "Generation of attosecond light pulses from gas and solid state media," Photonics **4**, 26 (2017).
34. C. M. Heyl, H. Coudert-Alteirac, M. Miranda, M. Louisy, K. Kovacs, V. Tosa, E. Balogh, K. Varjú, A. L'Huillier, A. Couairon, and C. L. Arnold, "Scale-invariant nonlinear optics in gases," Optica **3**, 75–81 (2016).
35. D. E. Rivas, A. Borot, D. E. Cardenas, G. Marcus, X. Gu, D. Herrmann, J. Xu, J. Tan, D. Kormin, G. Ma, W. Dallari, G. D. Tsakiris, I. B. Földes, S.-W. Chou, M. Weidman, B. Bergues, T. Wittmann, H. Schröder, P. Tzallas, D. Charalambidis, O. Razskazovskaya, V. Pervak, F. Krausz, and L. Veisz, "Next generation driver for attosecond and laser-plasma physics," Sci. Rep. **7**, 5224 (2017).
36. A. Guggenmos, R. Rauhut, M. Hofstetter, S. Hertrich, B. Nickel, J. Schmidt, E. M. Gullikson, M. Seibald, W. Schnick, and U. Kleineberg, "Aperiodic CrSc multilayer mirrors for attosecond water window pulses," Opt. Express **21**, 21728–21740 (2013).
37. M. Schultze, B. Bergues, H. Schröder, F. Krausz, and K. L. Kompa, "Spatially resolved measurement of ionization yields in the focus of an intense laser pulse," New J. Phys. **13**, 033001 (2011).
38. G. Kolliopoulos, B. Bergues, H. Schröder, P. A. Carpeggiani, L. Veisz, G. D. Tsakiris, D. Charalambidis, and P. Tzallas, "Revealing quantum path details in high-field physics," Phys. Rev. A **90**, 013822 (2014).
39. N. Tsatrafyllis, B. Bergues, H. Schröder, L. Veisz, E. Skantzakis, D. Gray, B. Bodi, S. Kuhn, G. D. Tsakiris, D. Charalambidis, and P. Tzallas, "The ion microscope as a tool for quantitative measurements in the extreme ultraviolet," Sci. Rep. **6**, 21556 (2016).
40. D. M. P. Holland, K. Codling, G. V. Marr, and J. B. West, "Multiple photoionization in the rare gases from threshold to 280 eV," J. Phys. B **12**, 2465–2484 (1979).
41. B. Gstir, S. Denifl, G. Hanel, M. Rümmele, T. Fiegele, P. Cicman, M. Stano, S. Matejcik, P. Scheier, K. Becker, A. Stamatovic, and T. D. Märk, "Electron impact multiple ionization of neon, argon and xenon atoms close to threshold: appearance energies and Wannier exponents," J. Phys. B **35**, 2993–3007 (2002).
42. R. Guichard, M. Richter, J.-M. Rost, U. Saalmann, A. A. Sorokin, and K. Tiedtke, "Multiple ionization of neon by soft x-rays at ultrahigh intensity," J. Phys. B **46**, 164025 (2013).
43. A. S. Kheifets, "Sequential two-photon double ionization of noble gas atoms," J. Phys. B **40** F313–F318 (2007).
44. A. Karamatskou, "Nonlinear effects in photoionization over a broad photon-energy range within the TDCIS scheme," J. Phys. B **50**, 013002 (2017).
45. B. Kämmerling, B. Krässig, and V. Schmidt, "Direct measurement for the decay probabilities of 4dj hole states in xenon by means of photoelectron-ion coincidences," J. Phys. B **25**, 3621–3629 (1992).
46. F. Penent, J. Palaudoux, P. Lablanquie, L. Andric, R. Feifel, and J. H. D. Eland, "Multielectron spectroscopy: the xenon 4d hole double Auger decay," Phys. Rev. Lett. **95**, 083002 (2005).
47. M. Uiberacker, T. Uphues, M. Schultze, A. J. Verhoef, V. Yakovlev, M. F. Kling, J. Rauschenberger, N. M. Kabachnik, H. Schröder, M. Lezius, K. L. Kompa, H.-G. Muller, M. J. J. Vrakking, S. Hendel, U. Kleineberg, U. Heinzmann, M. Drescher, and F. Krausz, "Attosecond real-time observation of electron tunneling in atoms," Nature **446**, 627–632 (2007).
48. S. X. Hu and L. A. Collins, "Attosecond pump probe: exploring ultrafast electron motion inside an atom," Phys. Rev. Lett. **96**, 073004 (2006).
49. S. Kühn, M. Dumergue, S. Kahaly, S. Mondal, M. Füle, T. Csizmadia, B. Farkas, B. Major, Z. Várallyay, E. Cormier, M. Kalashnikov, F. Calegari, M. Devetta, F. Frassetto, E. Månsson, L. Poletto, S. Stagira, C. Vozzi, M. Nisoli, P. Rudawski, S. Maclot, F. Campi, H. Wikmark, C. L. Arnold, C. M. Heyl, P. Johnsson, A. L'Huillier, R. Lopez-Martens, S. Haessler, M. Bocoum, F. Boehle, A. Vernier, G. Iaquaniello, E. Skantzakis, N. Papadakis, C. Kalpouzos, P. Tzallas, F. Lépine, D. Charalambidis, K. Varjú, K. Osvay, and G. Sansone, "The ELI-ALPS facility: the next generation of attosecond sources," J. Phys. B **50**, 132002 (2017).